JOURNAL OF THEORETICAL
AND APPLIED MECHANICS
3, **39**, 2001

CONTACT PROBLEMS WITH FRICTION, ADHESION AND WEAR IN ORTHOPAEDIC BIOMECHANICS. PART II – NUMERICAL IMPLEMENTATION AND APPLICATION TO IMPLANTED KNEE JOINTS

Jerzy Rojek
Józef Joachim Telega
Stanisław Stupkiewicz

Institute of Fundamental Technological Research, Warsaw
e-mail: jrojek@ippt.gov.pl; jtelega@ippt.gov.pl; sstupkie@ippt.gov.pl

The present paper is the second part of the contribution by Rojek and Telega (2001). An alternative adhesion law was used to the study of bone-implant interface. Numerical scheme was developed and applied to the knee joint after arthroplasty. Influence of wear debris on this interface and currently used wear models were investigated.

Key words: unilateral contact, adhesion, friction, wear, knee joint after arthroplasty, FEM

1. Introduction

In the first part of the paper, a general model of adhesion with friction and generalized unilateral contact conditions was developed for two deformable bodies, within the range of small deformations. Such a model applies to not necessarily linear elastic bodies. However, having in mind application to orthopaedic biomechanics, only linear elastic solids have been considered.

In the second part of the paper we develop a numerical implementation for unilateral contact problems with friction and adhesion, see Sections 2-4. Particularly, in Section 2 a general form of finite element equations is given. Section 3 is concerned with regularization of contact constraints. Numerical contact algorithm is elaborated in Section 4. In Section 5 we first test the developed numerical algorithm and next, perform the analysis of proximal tibia after total knee replacement (TKR). The last section deals with wear in

joints after arthroplasty. Currently used phenomenological models of wear are also discussed.

2. Finite element equations

Introducing space discretization of displacements

$$\boldsymbol{u}(t,\boldsymbol{x}) = \boldsymbol{N}(\boldsymbol{x})\boldsymbol{a}(t) \tag{2.1}$$

to the set of differential equations from Part I (Rojek and Telega, 2001) and applying the standard finite element procedure based on the Galerkin method, cf Zienkiewicz and Taylor (1998), we obtain the following set of semi-discrete equations of motions

$$\mathbf{M}\ddot{\boldsymbol{a}} = \boldsymbol{F}_{ext} + \boldsymbol{F}_c - \boldsymbol{F}_{int} \tag{2.2}$$

which are the basis of the explicit dynamic formulation. In the above equations $\mathbf{N}$ is the matrix of interpolation functions, $\boldsymbol{a}$ and $\ddot{\boldsymbol{a}}$ are the vectors of nodal displacements and accelerations, respectively, $\mathbf{M}$ is the mass matrix, $\boldsymbol{F}_{ext}$, $\boldsymbol{F}_{int}$ and $\boldsymbol{F}_c$ are the vectors of external loads, internal and contact forces, respectively. The vectors and matrices in Eq. (2.2) are defined as follows

$$\begin{aligned}
\mathbf{M} &= \int_{\Omega} \rho \mathbf{N}^{\top}\mathbf{N}\, d\Omega \\
\boldsymbol{F}_{ext} &= \int_{\Omega} \mathbf{N}^{\top}\boldsymbol{f}\, d\Omega + \int_{\Gamma_1} \mathbf{N}^{\top}\boldsymbol{g}\, d\Gamma \\
\boldsymbol{F}_{int} &= \int_{\Omega} \mathbf{B}^{\top}\boldsymbol{\sigma}\, d\Omega
\end{aligned} \tag{2.3}$$

where $\boldsymbol{\sigma}$ is the Cauchy stress tensor, $\mathbf{B}$ is the strain-displacement operator matrix, $\boldsymbol{g}$ is the vector of prescribed traction, $\boldsymbol{f}$ is the vector of given body forces. Calculation of nodal contact forces $\boldsymbol{F}_c$ will be explained later on.

Equations (2.2) are integrated in time using an explicit scheme, in which the displacements $\boldsymbol{a}^{k+1}$ at time t^{k+1} are obtained from the equations for the known configuration at time t^k

$$\begin{aligned}
&\ddot{\boldsymbol{a}}^k = \mathbf{M}_D^{-1}\left(\boldsymbol{F}_{ext}^k + \boldsymbol{F}_c^k - \boldsymbol{F}_{int}^k\right) && \mathbf{M}_D = \operatorname{diag}\mathbf{M} \\
&\dot{\boldsymbol{a}}^{k+1/2} = \dot{\boldsymbol{a}}^{k-1/2} + \ddot{\boldsymbol{a}}^k \Delta t^{k+1/2} && \Delta t^{k+1/2} = \frac{1}{2}(\Delta t^k + \Delta t^{k+1}) \\
&\boldsymbol{a}^{k+1} = \boldsymbol{a}^k + \dot{\boldsymbol{a}}^{k+1/2}\Delta t^{k+1}
\end{aligned} \tag{2.4}$$

Now the superscript k denotes that a variable is taken at instant t^k. The effectiveness of the explicit dynamic formulation is based on the use of a diagonal mass matrix $\mathbf{M}_D$, so there is no need to solve a system of equations. The main disadvantage is the limitation of the time step size Δt due to the conditional stability of the integration scheme.

The new contact formulation has been implemented within the dynamic explicit formulation in the finite element program Simpact (Rojek et al., 1998). Because of its efficiency in the analysis of large-scale systems the dynamic explicit approach has become very popular in many applications, cf Rojek et al. (1998), Chenot and Bay (1998).

The explicit dynamic codes are best suited to carry out simulation of dynamic processes, nevertheless they can be applied to quasi-static simulation as well. We can obtain approximate solutions of linear and non-linear quasi-static problems introducing adequate damping which would damp out the oscillations. Adding the damping term to Eq. (2.2) we have

$$\mathbf{M}\ddot{\boldsymbol{a}} + \mathbf{C}\dot{\boldsymbol{a}} = \boldsymbol{F}_{ext} + \boldsymbol{F}_c - \boldsymbol{F}_{int} \tag{2.5}$$

where $\mathbf{C}$ is the damping matrix and $\dot{\boldsymbol{a}}$ is the vector of nodal velocities.

Usually it is sufficient to damp out the lowest vibration modes. This can be achieved by applying global viscous damping close to the critical value for the lowest frequencies. The loading velocity should correspond to the dynamic properties of the system as well, and it should be introduced for a time sufficiently long in comparison to the period of vibrations in the lowest natural mode. Using this methodology we have performed the analysis of total knee replacement subjected to quasi-static loading, presented in Section 5.

Dynamic relaxation, a methodology elaborated to analyse quasi-static problems with dynamic model is presented by Underwood (1983). For survey papers on finite element method in biomechanics the reader is referred to Mackerle (1998) and Prendergast (1997), cf also Joshi et al. (2000), Rakotomanana (2000).

3. Regularization of contact constraints

The complete set of contact conditions that must be taken into account consists of the conditions for normal contact with adhesion, cf Rojek and Telega (2001)

$$u_n \geqslant 0 \qquad -R_n^e + k_n u_n \beta^2 \geqslant 0 \qquad (-R_n^e + k_n u_n \beta^2) u_n = 0 \tag{3.1}$$

relations for tangential contact with adhesion and friction

$$\begin{aligned} &\boldsymbol{R}_T^e = k_T \boldsymbol{u}_T \beta^2 \\ &\phi \leqslant 0 \qquad \lambda \geqslant 0 \qquad \phi\lambda = 0 \\ &\dot{\boldsymbol{u}}_T + \lambda \boldsymbol{R}_T^i = \boldsymbol{0} \end{aligned} \tag{3.2}$$

where

$$\phi = \|\boldsymbol{R}_T^i\| - \mu|R_n - k_n u_n \beta^2| \tag{3.3}$$

as well as the evolution law for the adhesion intensity β given by relations

$$\begin{aligned} \dot{\beta} &= -\Big\{-\frac{1}{b}[w - (k_n u_n^2 + k_T \|\boldsymbol{u}_T\|^2)\beta]^-\Big\}^{1/p} \qquad \text{if} \quad \beta \in [0,1[\\ \dot{\beta} &\leqslant -\Big\{-\frac{1}{b}[w - (k_n u_n^2 + k_T \|\boldsymbol{u}_T\|^2)]^-\Big\}^{1/p} \qquad \text{if} \quad \beta = 1 \end{aligned} \tag{3.4}$$

Regularization of contact constraints simplifies the variational formulation of the contact problem. Here we shall apply the penalty method to enforce the constraints for normal and tangential constraints.

The regularization of the normal contact conditions (3.1) is accomplished by introducing the penalty coefficient k_n^-. The impenetrability condition is enforced by

$$R_n^- = k_n^- u_n^- \tag{3.5}$$

where R_n^- and u_n^- stand for the negative parts of R_n and u_n, respectively (zero irreversible normal traction is taken into account here). The relation (3.5) applies to compression only, the relations for adhesive traction

$$R_n = k_n u_n \beta^2 \qquad \text{if} \quad u_n > 0 \tag{3.6}$$

remains unchanged. For consistency in notation, however, we shall rewrite it as

$$R_n^+ = k_n^+ u_n^+ \beta^2 \tag{3.7}$$

where R_n^+ and u_n^+ stand for the nonnegative parts of R_n and u_n, respectively.

The above modifications should be taken into account in Eq. (3.6), which now takes the form

$$\phi = \|\boldsymbol{R}_T^i\| - \mu|R_n^-| \tag{3.8}$$

The regularization of frictional constraints is carried out by introducing into Eq. $(3.2)_3$ the friction tangential penalty coefficient ε_T

$$\dot{\boldsymbol{u}}_T + \lambda \boldsymbol{R}_T^i = \frac{1}{\varepsilon_T} \dot{\boldsymbol{R}}_T^i \tag{3.9}$$

where $\dot{\boldsymbol{R}}_T^i$ is the time derivative of $\boldsymbol{R}_T^i$. For large displacement formulation the Lie derivative should be used here, cf Laursen and Simo (1993). The regularization becomes exact as $\varepsilon_T \to \infty$.

Penalization of normal and tangential contact constraints is equivalent to specifying additional constitutive relations on the interface. Thus the elastic behaviour has been introduced here for compression in normal contact, and the frictional contact has been reformulated as a problem analogous to that of elastoplasticity, the elastic component of tangential velocity being specified by $(1/\varepsilon_T)\dot{\boldsymbol{R}}_T^i$.

Regularized contact conditions constitute the basis of the numerical algorithm for the calculation of contact interaction forces.

4. Numerical contact algorithm

At every step of the time integration the contact algorithm performs two basic tasks:

- contact search to establish the contact area,
- evaluation of contact forces.

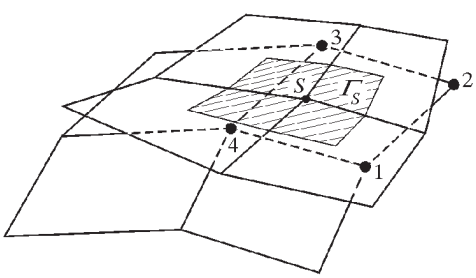

Fig. 1. Discretized contact surfaces

The contact search in the implemented finite element algorithm is carried out by checking the location of the points discretizing one of the two surfaces, called "slave", with respect to the other one, called "master" (see Fig. 1). In the standard contact algorithm (without adhesion), contact is established for the slave nodes penetrating through the master surface $(u_n < 0)$. In the present algorithm the contact search has been modified to include the possibility of adhesive contact $(u_n > 0)$.

Once the contact is established between a certain slave node S and a master segment defined with nodes 1 through 4 (Fig. 1) at time t^k, the relative displacements u_n^k and $\boldsymbol{u}_T^k$, the tangential relative velocity $\dot{\boldsymbol{u}}_T^k$ are obtained. Given these variables and interface constitutive parameters, k_n^-, k_n^+, k_T, w, μ, b and p, the contact interactions R_n^k and $\boldsymbol{R}_T^k$, and intensity of adhesion β^k are calculated. Previous values of irreversible tangential force $(\boldsymbol{R}_T^i)^{k-1}$ and intensity of adhesion β^{k-1} are required to calculate new state at the contact interface.

The contact force applied to the node S is obtained by integrating the contact traction R_n^k and $\boldsymbol{R}_T^k$ over a part of the boundary Γ_S associated with the node S (see Fig. 1)

$$(\boldsymbol{F}_c^k)_S = (R_n^k \boldsymbol{n} + \boldsymbol{R}_T^k)|\Gamma_S| \tag{4.1}$$

$|\Gamma_S|$ – surface measure of Γ_S.

The reaction applied to the master surface is next replaced by equivalent forces applied to the master segment nodes 1 through 4

$$(\boldsymbol{F}_c^k)_i = -N_i(\boldsymbol{F}_c^k)_S \qquad i = 1, \ldots, 4 \tag{4.2}$$

where N_i is the shape function corresponding to the ith node at the projection of the slave node S on the master segment.

The numerical algorithm used to calculate the state of the contact interface is summarized below as follows:

1. *Evolution of intensity of adhesion*

   If $\beta^{k-1} > 0$ (if adhesion bonds exist), a trial value of $\dot{\beta}^k$ is calculated using relation $(3.4)_1$

   $$\dot{\beta}_{trial}^k = -\Big\{-\frac{1}{b}\Big[w - \Big(k_n^+ \big(u_n^{(+)k}\big)^2 + k_T \|\boldsymbol{u}_T^k\|^2\Big)\beta^{k-1}\Big]\Big\}^{1/p} \tag{4.3}$$

   Normal contact force contribution is taken into account in Eq. (4.3) for tensile interface traction only. If $\dot{\beta}_{trial}^k < 0$, we have a decohesion process and a new value of the intensity of adhesion is calculated using forward Euler scheme

   $$\beta^k = \beta^{k-1} + \dot{\beta}_{trial}^k \Delta t^k \tag{4.4}$$

   otherwise we set

   $$\beta^k = \beta^{k-1} \tag{4.5}$$

2. *Normal contact force*

If $u_n^k \leqslant 0$ the compressive traction is calculated from Eq. (3.5)

$$R_n^k = k_n^- u_n^k \tag{4.6}$$

otherwise the tensile traction due to adhesion is calculated from Eq. (3.7)

$$R_n^k = k_n^+ u_n^k (\beta^k)^2 \qquad \text{if} \quad \beta^k > 0 \tag{4.7}$$

or R_n^k is set to zero

$$R_n^k = 0 \qquad \text{if} \quad \beta^k = 0 \tag{4.8}$$

3. *Adhesive tangential contact force*

Adhesive tangential contact traction is calculated from Eq. $(3.2)_1$

$$(\boldsymbol{R}_T^e)^k = k_T \boldsymbol{u}_T^k (\beta^k)^2 \qquad \text{if} \quad \beta^k > 0 \tag{4.9}$$

or $(\boldsymbol{R}_T^e)^k$ is set to zero, if adhesion is absent

$$(\boldsymbol{R}_T^e)^k = \boldsymbol{0} \qquad \text{if} \quad \beta^k = 0 \tag{4.10}$$

4. *Frictional tangential contact force*

For tensile normal contact traction $(R_n > 0)$ the friction force is set to zero

$$(\boldsymbol{R}_T^i)^k = \boldsymbol{0} \tag{4.11}$$

If the normal contact traction is compressive, the friction contact traction is calculated using the radial return algorithm analogous to that used in elastoplasticity. First we calculate a trial state employing Eqs. (3.9)

$$(\boldsymbol{R}_T^i)_{trial}^k = (\boldsymbol{R}_T^i)^{k-1} + \varepsilon_T \dot{\boldsymbol{u}}_T^k \Delta t^k \tag{4.12}$$

and check the slip condition (3.8)

$$\phi_{trial} = \|(\boldsymbol{R}_T^i)_{trial}^k\| - \mu |R_n^k| \tag{4.13}$$

If $\phi_{trial} \leqslant 0$, we have the case of stick contact and the frictional traction is assigned the trial value

$$(\boldsymbol{R}_T^i)^k = (\boldsymbol{R}_T^i)_{trial}^k \tag{4.14}$$

otherwise (slip contact) we perform a return map

$$(\boldsymbol{R}_T^i)^k = \mu |R_n^k| \frac{(\boldsymbol{R}_T^i)_{trial}^k}{\|(\boldsymbol{R}_T^i)_{trial}^k\|} \tag{4.15}$$

Thus we have the state of the contact interface completely defined. The above algorithm takes into account all possible loading, unloading and reloading conditions which will be demonstrated in an example in the next section. The intensity of adhesion in the present formulations tends to zero $(\beta \to 0)$ as the process of decohesion continues, but never achieves zero. For practical handling of cases with adhesive bonds broken we have introduced a small limit value β_{min}, below which we assume that the adhesion disappears, and then we set $\beta = 0$.

5. Numerical examples

The aim of this section is twofold. First, we will test only the elaborated numerical algorithm for contact problem with adhesion and friction. Second, the discretized interface model will be applied to the analysis of proximal tibia after TKR.

5.1. Study of a contact interface under different loading conditions

We analyze a contact interface in 2D with different properties and under different loading conditions. Using the developed routines we calculate the contact forces under prescribed relative displacements. In the first case we analyze the normal behaviour of a contact interface with adhesion with the following properties: $k_n = 20\,\mathrm{kPa/mm}$, $w = 2\,\mathrm{kJ/mm^2}$, $p = 1$. The loading was imposed by the constant velocity $\dot{u}_n = 2\,\mathrm{mm/s}$, $t \in [0, 0.2]\,\mathrm{s}$. We have analyzed the interface for different viscosity: $b = 1 \cdot 10^{-4}$, $1 \cdot 10^{-2}$, $5 \cdot 10^{-2}$ and $1 \cdot 10^{-1}\,\mathrm{kN{\cdot}s/mm}$. We start from the total adhesion $(\beta = 1)$ and zero displacement $(u_T = u_n = 0)$. Figure 2 depicts the normal force history obtained for these conditions. We can see that until the elasticity energy is smaller than the limit of adhesion energy, the force increases linearly. After passing this limit adhesion starts to decrease, although for higher values of viscosity the adhesion force can be higher than the limit resulting from the limit of adhesion energy. The higher the value of viscosity b, the longer will be the delay in the adhesion force decrease. Finally the interfacial force decreases nearly to zero, what means that the adhesion bonds are nearly broken.

The same interface was loaded with prescribed velocity $\dot{u}_n = 2\,\mathrm{mm/s}$ for $t \in [0, 0.1]\,\mathrm{s}$, then unloaded $-\dot{u}_n = -2\,\mathrm{mm/s}$ for $t \in [0.1, 0.15]\,\mathrm{s}$, and loaded $-\dot{u}_n = 2\,\mathrm{mm/s}$ for $t \in [0.15, 0.3]\,\mathrm{s}$. The problem was studied for two values of viscosity: $b = 1 \cdot 10^{-4}$ and $1 \cdot 10^{-1}\,\mathrm{kN{\cdot}s/mm}$. The results in the form

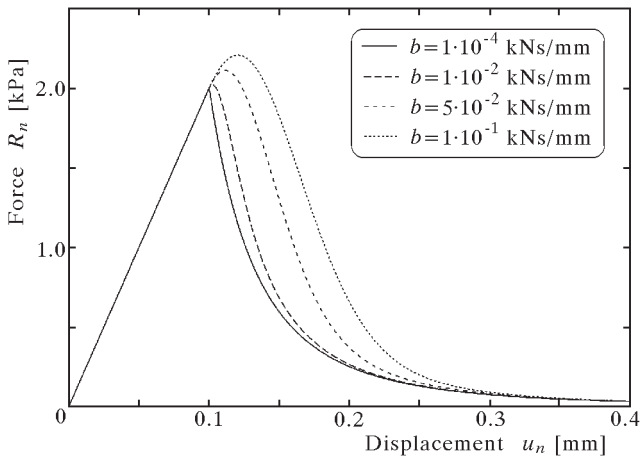

Fig. 2. Adhesion force for different viscosity

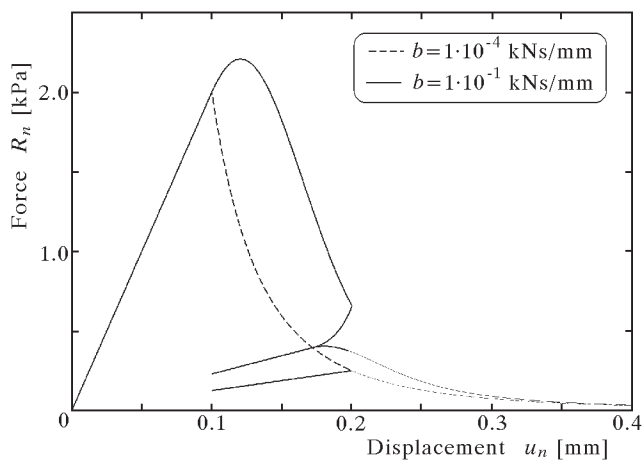

Fig. 3. Adhesion force for different viscosity under loading and unloading

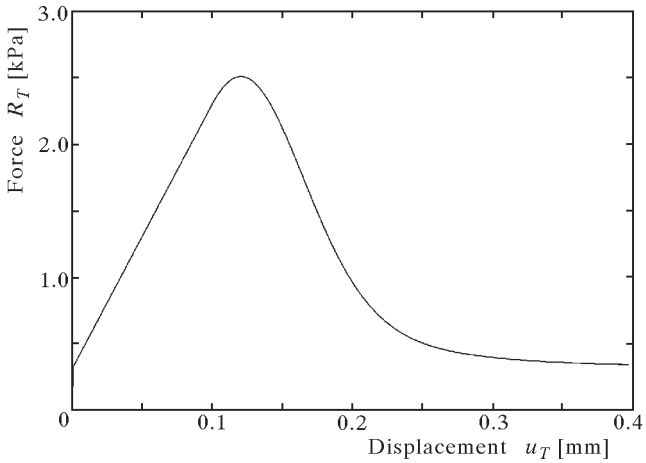

Fig. 4. Tangential force for adhesion with friction

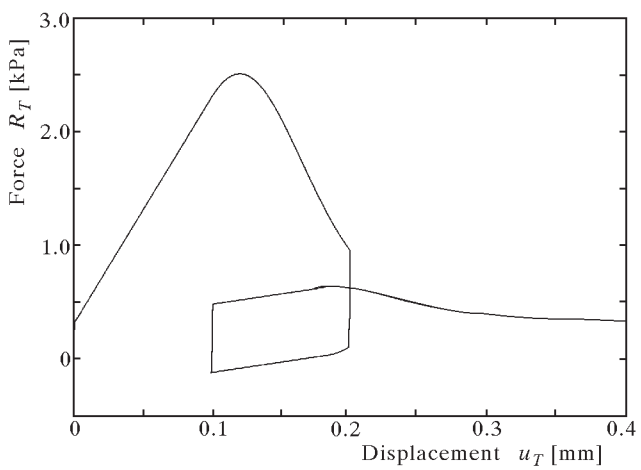

Fig. 5. Tangential force for adhesion with friction under loading and unloading

of relation adhesion force vs. relative displacement are shown in Fig. 3. We can see the unloading for the stiffness of the adhesion decreased. We can also see the viscous effect in unloading for higher value of the viscosity. It is thus shown that the adhesive bonds can keep breaking even during unloading if the viscosity is present.

We analyze the tangential behaviour of a contact interface with adhesion and friction The interface has the following properties: $k_n^- = k_T = 20\,\mathrm{kPa/mm}$, $w = 2\,\mathrm{kJ/mm^2}$, $b = 1 \cdot 10^{-1}\,\mathrm{kN{\cdot}s/mm}$, $p = 1$, $\mu = 0.3$. The loading was imposed by the constant velocity $\dot{u}_T = 2\,\mathrm{mm/s}$, $t \in [0, 0.2]\,\mathrm{s}$. Constant compression was applied by setting constant normal displacement $u_n = -0.5\,\mathrm{mm}$. Figure 4 presents the tangential force history obtained. We can see that tangential force has the frictional component equal to the sliding limit μR_n. The tangential force after breaking adhesive bonds tends to the sliding limit now.

The same interface was loaded with the imposed velocity according to the following program: $\dot{u}_n = 2\,\mathrm{mm/s}$ for $t \in [0, 0.1]\,\mathrm{s}$, $\dot{u}_n = 0$ for $t \in [0.1, 0.11]\,\mathrm{s}$, $\dot{u}_n = -2\,\mathrm{mm/s}$ for $t \in [0.11, 0.16]\,\mathrm{s}$, $\dot{u}_n = 2\,\mathrm{mm/s}$ for $t \in [0.16, 0.31]\,\mathrm{s}$. Figure 5 represents the tangential force history obtained. We can see that when the loading is constant, the adhesion keeps decreasing because of relaxation. Under unloading conditions the adhesive and friction forces have opposite orientation. Under reloading the sign of friction force is changed and again is the same as that of the adhesion component. When adhesion disappears, the tangential force is equal to the sliding limit.

The examples analyzed here demonstrate correctness of the formulation and numerical algorithm. The friction and adhesion forces have been calculated correctly under different complex loading. This verification allows us to use the numerical algorithm for real problems of contact with adhesion and friction.

5.2. Analysis of adhesion in the total knee replacement

We apply the interface model with adhesion to an analysis of proximal tibia after TKR. Fixation of prosthesis is one of the most important mechanical aspects of the performance of the bone-implant system. As we already know, loosening can be caused by variety of mechanical and biological phenomena, cf Sections 2, 3 in Rojek and Telega (2001) and Section 6 which follows. In the present analysis we shall study loosening of a cemented stem initiated by debonding at the stem-cement interface, and we shall focus on the role of adhesion in the fixation of implants.

The knee experiences an oscillating varus-valgus loading. Off-centered load can cause tensile stresses on the knee implant interfaces (Fig. 6). Cement has

poor tensile properties, therefore debonding can occur under tension. One of the design objective of a knee implant is avoidance of the interface tension.

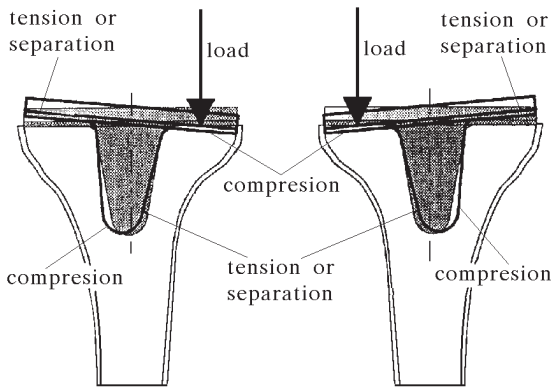

Fig. 6. Interface tension and compression in the knee implant under off-centred loading

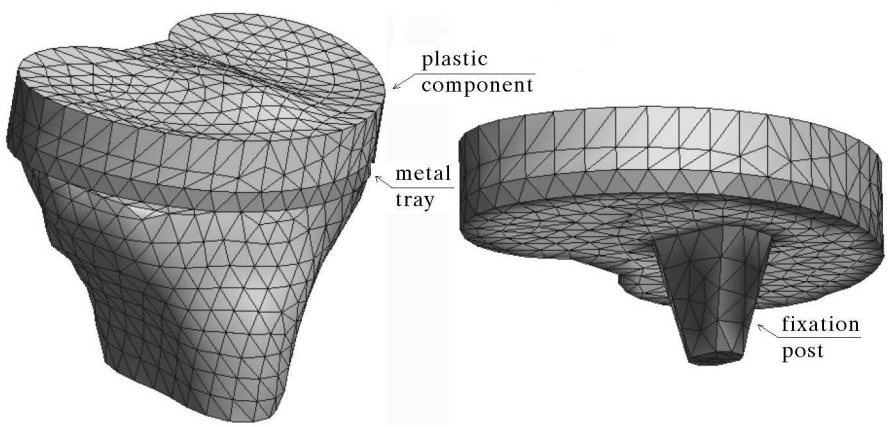

Fig. 7. Finite element model of tibia with implant

The proximal tibia with mounted tibial component of the condylar replacement has been discretized with tetrahedral finite elements (Fig. 7). The tibial component of the endoprosthesis has a plastic bearing surface placed on a metal tray with central cemented post. Isotropic elastic properties for the materials in the model have been assumed as follows:

- cortical bone: Young's modulus $1.7 \cdot 10^{10}$ Pa, Poisson's ratio 0.32,
- cement: Young's modulus $2.27 \cdot 10^{9}$ Pa, Poisson's ratio 0.335,

- steel: Young's modulus $2.14 \cdot 10^{11}$ Pa, Poisson's ratio 0.30,
- polyethylene: Young's modulus $1 \cdot 10^{9}$ Pa, Poisson's ratio 0.30.

Contact with adhesion and friction has been taken into account at the steel-bone and steel-cement interfaces, while materials at other interfaces have been considered to be fully bonded. The following properties have been assumed for all the interfaces with adhesion:

- interface normal stiffness $k_n = k_n^- = 1 \cdot 10^{12}$ Pa/m,
- interface tangential stiffness $k_T = 1 \cdot 10^{11}$ Pa/m,
- energy of adhesion $w = 0.36\,\mathrm{J/m^2}$,
- viscosity parameter $b = 0$,
- Coulomb friction coefficient $\mu = 0.1$.

The above interface properties yield the limit tensile stress 0.6 MPa at the separation $0.6 \cdot 10^{-3}$ mm, and the limit shear interface strength 0.19 MPa at the tangential relative displacement $1.9 \cdot 10^{-3}$ mm (friction, however, raises total tangential resistance). These properties correspond to a relatively weak interface strength, weaker than that of real bonding. Such an assumption, however, was necessary to allow the interface to debond.

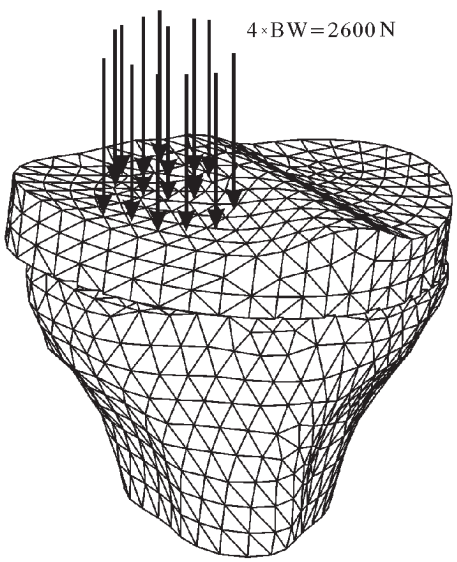

Fig. 8. Finite element model with loading condition

The tibia has been fixed distally at the base of the bone and the loading has been applied non-symmetrically on the bearing surface (Fig. 8). The load

condition approximated a tibio-femoral contact forces in one leg standing position. The compressive force of 400% BW (body weight) has been assumed. For BW = 700 N we have $R_{max} = 2600$ N. The force has been distributed over the supposed contact area between tibial and femoral comoponents.

Quasi-static loading has been analyzed using dynamic relaxation method. Loading has been growing linearly from 0 to the final value of 400% BW. The quasi-static behaviour has been obtained by introducing adequate (close to critical) damping. Distribution of stresses in the tibia with implant under the loading of 320% BW is shown in Fig. 9b. Figure 9a shows the displacement vectors for the same level of loading; it can be clearly seen that the side of the tray opposite to the loading is raised. This causes tensile contact tractions.

Evolution of interface normal stresses on the tray and stem surfaces is shown in Fig. 10. Evolution of tangential contact stresses is shown in Fig. 11. The decohesion process can be analyzed studying the evolution of the intensity of adhesion β, cf Fig. 12.

The results in Figs. 10-12 are presented for the bonded area only, the reduction of this area corresponds to the decohesion process. Initially we have bonding at the whole surface. Until certain level of loading the bonding strength is not reached and the bonding is not broken. As we can see in Fig. 12, the bonded area up to 320% BW is practically not changed. For higher loads decohesion takes place. We can see that once decohesion has started, increasing loading leads quickly to to complete loosening of the prothesis.

6. Wear in implanted joints, wear models

Looking back, one should first mention ferrography, which was invented in the early 1970's and has gained use in the analysis of wear in machines, cf Evans et al. (1980). The ferrographic technique is based on the magnetic precipitation of particles from suspensions. In the papers by Evans (1983), Evans et al. (1980, 1981,1982), Mears et al. (1978), possibilities of employing the ferrography for the analysis of wear particles present in the synovial fluid aspirated from surgical joint replacements and human arthritic joints were examined.

Passing to recent results, a collection of papers contained in Dowson (1998) presents a good survey of experimental results on the subject of friction and wear of joint replacements and implant materials, cf also Saikko and Ahlroos (2000). Sophisticated single station machine simulators capable of measuring

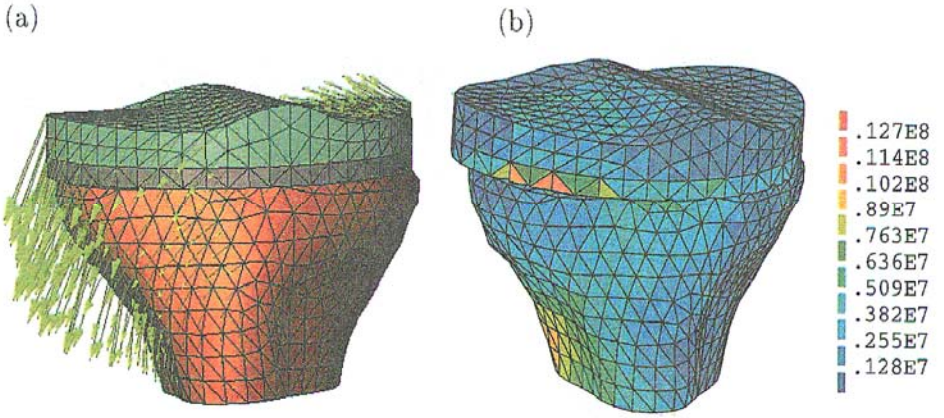

Fig. 9. Results of simulation for loading of 3.2 BW: (a) displacement vectors (500×geometry scale), (b) Huber-Mises stresses [Pa]

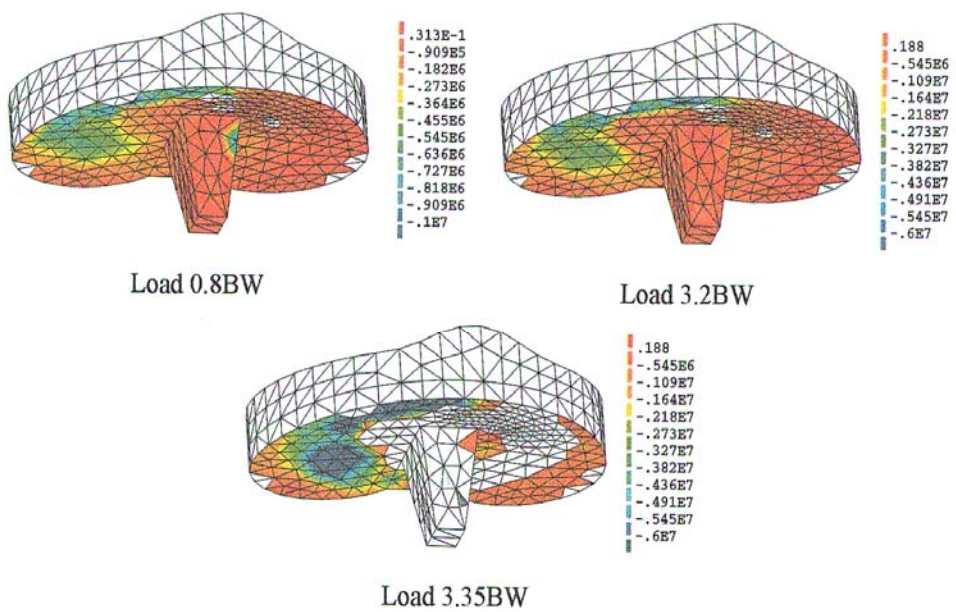

Fig. 10. Evolution of normal contact stresses [Pa], BW=2600 N

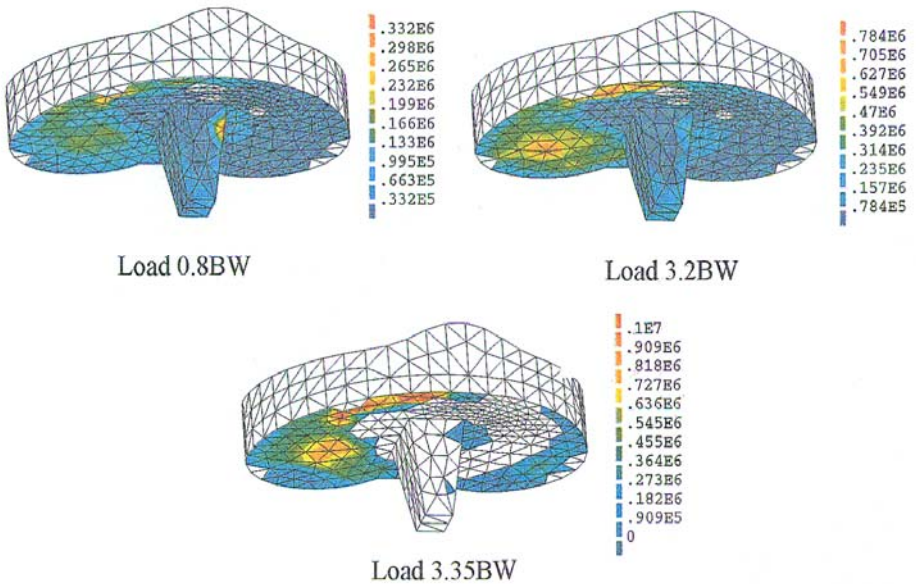

Fig. 11. Evolution of tangential contact stresses [Pa], BW=2600 N

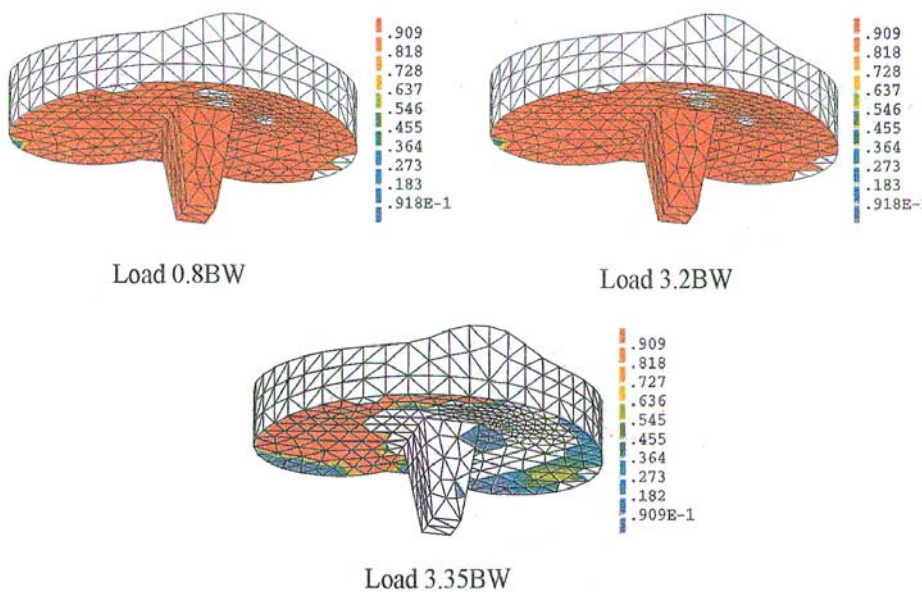

Fig. 12. Evolution of the coefficient of adhesion intensity β, BW=2600 N

both the wear and friction were also described, cf also Saikko (1993), Walker et al. (1997).

6.1. Basic wear effects

In the context of joint prostheses, there are two main groups of wear effects. The first group of problems is related to wear phenomena in the artificial joint and can be clasified as a mostly tribological problem when the contacting bodies are traditional materials, usually metal or ceramic and ultra-high molecular weight polyethylene (UHMWPE). However, even the implanted joint is lubricated by the synovial fluid, though not so effectively as natural healthy joints, cf Wang et al. (1998). The second group of problems is related to contact phenomena at bone-implant interfaces, cf the previous sections. In this case, one of the contacting bodies is a living tissue, thus several non-mechanical issues occur. The two tribological systems are strongly coupled, namely the UHMWPE wear debris is commonly agreed to be a major cause of long term failure of total joint replacement through aseptic loosening, cf Laffargue et al. (1998), Revell et al. (1997). Aseptic loosening is a process of prosthesis loosening due to bone loss in the absence of infection or mechanical failure. The bone loss process is induced by the inflamatory response to UHMWPE wear particles. A coupling effect in an opposite direction is also observed, namely the bone cement and bone particles originating from the bone-prosthesis interface may penetrate the joint and strongly accelerate the wear process due to the third body abrasion. Extensive experimental studies on friction and wear of ceramics were carried out by Sasaki (1992). However, a situation typical for ceramic bone implants was not investigated.

For these reasons, the study of the two tribological systems and their relative coupling is an important area of biomechanics. Many efforts have been concentrated on experimental studies of wear performance of UHMWPE by means of traditional pin-on-disk devices (Klapperich et al., 1999; Saikko and Ahlroos, 2000), special joint simulators (Saikko, 1993) and analysis of explanted joints after *in vivo* operation (Atkinson et al., 1985). Dowson (1998) and Wang et al (1998) provide extensive reviews of the recent advances in the tribology of artificial joints. For instance, topics such as the major wear mechanisms and lubrication regimes, effects of surface roughness and joint kinematics on wear mechanisms are discussed in the paper by Wang et al. (1998).

Wear particles of different materials are found in the cells next to the loosened artificial joint prostheses, but also in distant locations, such as liver, spleen and kidney (Revell et al., 1997). The transport of particles by the host defense mechanisms is affected by the particle material, size and shape,

therefore it is not only the wear volume that is important, but also the size and shape of wear particles generated at contact interfaces, cf Dowson (1998). Clearly, with decreasing size the number of particles per unit wear volume increases. In fact, the particle size may vary from 0.2 μm to 100 μm, cf Ingham and Fischer (1999), which may lead to a several orders of magnitude difference in the number of particles for a fixed wear volume.

6.2. Models of plasticity-determined wear mechanisms

There are three main basic wear mechanisms occuring at artificial joint interfaces, namely adhesive wear, abrasive wear and surface fatigue wear (Wang et al., 1998). According to Lim and Ashby (1987), the adhesive and abrasive (and also to some extent fatigue) wear mechanisms are *plasticity-determined*. Adhesive wear is explained by welding at asperity contacts followed by removal of shearing (due to sliding) of softer asperity fragments which can further create wear particles, cf Archard (1953). Abrasive wear is caused by hard asperities or particles (two- or three-body abrasive wear) ploughing the softer surface. This is accompanied by severe plastic deformation of the subsurface layer. In some cases (e.g. hard and sharp particles) ploughing can cause chip cutting, thus leading to direct formation of wear particles but more often wear results from repeated plastic deformation and micro-crack propagation.

Wear due to fatigue is caused by crack propagation caused by repeated cyclic loading of the surface. This can occur on the macro-level, as in rolling contact, or on micro-level due to multiple asperity contacts during sliding. The latter case is often recalled when discussing adhesive or abrasive wear mechanisms since wear rates resulting from assumption that every asperity contact produces wear particle are several orders of magnitude higher than those observed experimentally.

Despite the fundamental differences betwen the different wear mechanisms (and respective friction mechanisms) they have the plastic deformation origin in common. Since the microscopic plastic deformation in the subsurface layer is a manifestation of the macroscopic phenomenon of friction, the corresponding dissipation rates are directly related. Therefore, the plasticity-determined wear mechanisms are well described by the Archard wear law, which predicts the wear rate to be proportional to the frictional dissipation rate. Of course, depending on the contact conditions (surface roughness, range of contact pressures, lubrication regime, etc.) different friction and wear mechanisms may be active for the same pair of contacting materials and each mechanism may be characterized by a different proportionality factor of the wear law.

Below, the classical model of adhesive wear of Archard (1953) is outlined

and the wear law is derived. Next, the delamination theory of wear is briefly presented, as it seems much relevant for description of wear phenomena at the contact interfaces in joint prostheses.

6.2.1. Archard law of adhesive wear

A simple model of adhesive wear has been proposed by Archard (1953). Assuming that wear particles created at single asperity contacts have similar shapes and their size is characterized by the diameter a of single real contact areas, the volume of the wear particle is proportional to a^3. Further, assuming that the sliding distance over which the wear particle is formed equals the contact area diameter a (after sliding this distance, the next asperity takes the load) the volumetric wear rate W, i.e. the volume worn per unit sliding length, is proportional to the real contact area A

$$W \propto A$$

For moderate normal pressures a plastic contact of asperities occurs and the real contact area is proportional to the ratio of the normal load F_N and the hardness H of the softer body

$$A = \frac{F_N}{H} \tag{6.1}$$

So the wear rate per unit sliding length can be expressed as

$$W = \frac{KF_N}{H} \tag{6.2}$$

where K is the wear coefficient expressing the probability of a single asperity adhesive contact to form a wear particle. According to Archard's theory, the wear rate is proportional to the ratio of the normal force (or pressure) to the hardness of the softer material. The Archard's wear law is simple and turned to be valid in a wide range of sliding conditions, not only those characterized by asperity adhesion (see the following section).

In continuum mechanics it is more convenient to use rates with respect to time rather than to the sliding length and to use local variables (as the contact pressure p_N) rather than the global ones (as the normal force F_N). So the Archard's wear law (6.2) can be expressed in a local form

$$\dot{w} = \frac{kp_N v}{H} \tag{6.3}$$

where $\dot{w}$ denotes the depth of wear in unit time and v is the relative sliding velocity. Remind now that for the range of pressures for which the real area of

contact is proportional to normal pressure, cf Eq. (6.1), similar proportionality exists between the friction stress p_T and normal pressure p_N. The wear law (6.3) can be further rewritten to yield

$$\dot{w} = \frac{\widetilde{k}\dot{D}}{H} \tag{6.4}$$

where $\dot{D} = p_T v$ is the frictional dissipation rate and $\widetilde{k} = \mu k$ is the modified wear coefficient (μ denotes the friction coefficient).

6.2.2. Delamination theory of wear

It is easy to imagine material removal due to asperity shear-off or micro-cutting by a ploughing asperity. However, in many contact conditions those two mechanisms do not occur but the surfaces are still worn. The delamination theory of wear, originally developed for metals, explains another mechanism of material removal from contact surface during sliding, cf Suh (1973, 1977), by assuming void and micro-crack nucleation at some characteristic distance below the surface, as a result of plastic contact of single asperities, followed by crack propagation parallel to the surface and delamination of flake-like wear particles.

There are several facts justifying this mechanism. The mechanism of crack nucleation and propagation at some characteristic depth below the surface is explained by high compressive stresses which occur just below the contact regions. This depth is usually of the order of asperity size. Plastic deformation caused by a single pass of an asperity accumulates due to repeated action during sliding. Thus the voids are created around inclusions or due to dislocation pile-ups. Fracture mechanics analysis confirmed preferred direction of crack propagation in the plane parallel to the surface. Finally, the flake-like wear particles (with aspect ratio greatly different from unity) have been observed experimentally. An overview of the delamination theory of wear can be found in Suh (1977).

In order to show that the delamination theory of wear leads also to the wear law of the Archard's type we shall adopt the model developed by Lim and Ashby (1987). This model is quite simple and reflects the main ideas of Suh's model although it differs in some details.

Voids nucleate at inclusions at a characteristic depth X_0 due to repeated frictional traction on the sliding surface. The area fraction of voids f_A on a plane parallel to the sliding surface (at the depth X_0) is

$$f_A = (2r_i N_v)(2r_i)(2r_i\gamma) \approx 2f_v\gamma \tag{6.5}$$

where r_i is the inclusion radius, N_v is the number of inclusions per unit volume, γ is the cumulative plastic shear strain and f_v is the volume fraction of the inclusions. A critical value of area fraction $f_A = f_A^*$ is assumed to exist at which fracture causes a flake-like wear particle to break off. The critical shear strain associated with this fracture γ^* is then

$$\gamma^* = \frac{f_A^*}{2f_v} \tag{6.6}$$

and the number of passes n^* needed to build up γ^* follows from the plastic shear strain γ_0 accumulated per pass

$$\gamma^* = n^*\gamma_0 \tag{6.7}$$

The thickness of the wear flake that is created after n^* passes is X_0, so the wear rate is

$$W = \frac{X_0 A_n}{n^* d} \tag{6.8}$$

where A_n is the nominal area of contact and d is the asperity spacing. Using Eqs (6.6) and (6.7), the wear rate can be expressed as

$$W = \frac{2\gamma_0 f_v X_0}{f_A^* r_a}\frac{F_N}{H} \tag{6.9}$$

where the distance between asperity contacts d has been replaced by the equation

$$\frac{r_a}{d} = \frac{A_r}{A_n} = \frac{F_N}{H} \tag{6.10}$$

Here r_a is the radius of asperity contact, A_r and A_n denote real and nominal contact areas, respectively, F_N is the normal force and H is the hardness. Note that Eq. (6.10) is valid only for long wedge-like asperities (two-dimensional asperity model), cf Lim and Ashby (1987).

Finally, assuming that $X_0 = r_a$, what expresses the fact that the characteristic depth of crack nucleation and propagation is of the order of the asperity radius, the wear rate can be rewritten in the final form of Archard's law

$$W = \frac{2\gamma_0 f_v}{f_A^*}\frac{F_N}{H} \tag{6.11}$$

where the wear coefficient has been predicted as $K = 2\gamma_0 f_v / f_A^*$.

Remark 6.1. Strömberg et al. (1996a,b) developed a continuum thermodynamic model for interfacial phenomena including unilateral contact, friction and wear, cf also Mróz and Stupkiewicz (1994), Johansson (1992), Strömberg (1997). The model is confined to small displacements, implying small slip. A numerical model allowing for large slip was elaborated by Agelet de Saracibar and Chiumenti (1999), cf also Agelet de Saracibar (1997), Heegaard (1993), Heegaard and Curnier (1993), Laursen and Simo (1993). Only the Archard's law for adhesive wear was incorporated into the model developed by Agelet de Saracibar and Chiumenti (1999). A restricted class of initial-boundary value problems with friction and wear was studied by using methods of variational inequalities in Garcĭa et al. (2000), Kuttler and Shillor (1998), Shiller and Sofonea (1999). We observe that in none of the above approaches, the adhesion was included.

Remark 6.2. The study of contact problems in orthopaedic biomechanics requires models incorporating friction, adhesion and wear. However, wear debris are produced between different components of a prosthesis and different from the bone-implant interface; for instance between the tibial and femoral components of condylar TKR. In other words, one has to take into account the transport of wear debris to the interface where adhesion takes place. On such an interface a possible transport equation is

$$\frac{\partial C(x,t)}{\partial t} = \nabla \cdot \Big[\mathbf{a}(x)\nabla C(x,t) - C(x,t)\boldsymbol{v}(x,t)\Big] + R\Big(C(x,t)\Big) \tag{6.12}$$

Here $C(x,t)$ denotes the concentration of wear debris on the interface bone-implant, $\mathbf{a}$ is the matrix of diffusion coefficients, $\boldsymbol{v}$ is the (small) velocity of wear debris, R denotes the reaction term and t denotes time. Equation (6.12) has to be supplemented by the boundary and initial conditions.

7. Final remarks

Longevity of prosthesis depends on the quality of bone-implant interface. Though a lot of studies have been concerned with this subject, yet no general biomechanical model is available. Such a model should incorporate adhesion, friction and influence of wear debris. Then the density of adhesion would depend on the debris concentration $C(x,t)$, appearing in Eq. (6.12). We hope to cope with this problem in the future.

Bergmann and his coworkers developed experimental procedure for the determination of forces and friction-induced temperature in implanted hip joints, cf Bergmann et al. (1993, 1995, 1997, 1999), Graichen et al. (1999) and the references therein. Similar procedures has not yet been applied to knee joint after arthroplasty (G. Bergmann, private communication, 2000).

The review paper by Feeny et al. (1998), containing a comprehensive though not exhaustive list of references, provides an interesting historical overview of structural and mechanical systems with friction, beginning from the antiquity. However, striving for understanding the friction phenomenon in human and animal joints was overlooked.

Recently, a new idea of modelling friction was elaborated by Tworzydlo et al. (1998). These authors proposed an approach for constructing constitutive models of frictional interfaces, which provides a link between microscale phenomena and macroscale phenomenological models at the interface. Tworzydlo et al. (1998) claim that their micro-macro approach is based on statistical homogenisation. Unfortunately, this point remains unclear since no homogenisation problem was formulated.

Hip and knee implants are partially in contact with cancellous bone, which is a cellular solid, cf Gibson and Ashby (1988), Tokarzewski et al. (1999). Fortes et al. (1999) investigated the static contact of a cellular solid with open cells with a compact counter-surface. Such a model seems to be applicable to cancellous bone of rather low density in contact with a prosthesis, though obviously then the contact is much more complicated. Namely, according to Maher and McCormack (1999), the mechanical interlock created at the cement/cancellous bone interface in cemented femoral reconstruction is crucial to the longevity of the replacement. This interlock is created through fingers or pedicles of bone cement which protrude through cancellous trabecular spaces.

Another interesting idea is due to Zhang and Tanaka (1997), cf also the references therein. These authors studied the mechanisms of friction and wear on the atomic scale through the investigation of a typical diamond-copper sliding system with the aid of molecular dynamics analysis. However, one still lacks a theory bridging the gap between atomic analysis and that using continuum analysis. Sliding parts in a prosthesis usually consist of a pair made of UHMWPE-metal or UHMWPE-ceramics. Then it seems more appropriate to characterise the UHMWPE by its molecules.

Acknowledgment

The authors were supported by the State Committee for Scientific Research (KBN, Poland) through the grant No. 8 T11F 017 18. Thanks are given to Prof. Oñate from

the International Centre of Numerical Methods in Engineering in Barcelona for providing the numerical code Simpact.

References

1. Agelet de Saracibar C., 1997, A New Frictional Time Integration for Large Slip Multi-Body Frictional Contact Problems, *Comput. Meth. Appl. Mech. Eng.*, **142**, 303-334
2. Agelet de Saracibar C., Chiumenti M., 1999, On the Numerical Modeling of Frictional Wear Phenomena, *Comput. Meth. Appl. Mech. Eng.*, **177**, 401-426
3. Archard J.F., 1953, Contact and Rubbing of Flat Surfaces, *J. Appl. Phys.*, **24**, 981-988
4. Atkinson J.R., Dowson D., Isaac J.H., Wroblewski B.M., 1985, Laboratory Wear Tests and Clinical Observations of the Penetration of Femoral Heads into Acetabular Cups in Total Replacement Hip Joints III: The Measurement of Internal Volume Changes in Explanted Charnley Sockets after 2-16 Years *in Vivo* and the Determination of Wear Factors, *Wear*, **104**, 225-244
5. Bergmann G., Graichen F., Rohlmann A., 1993, Hip Joint Loading During Walking and Running, Measured in Two Patients, *J. Biomechanics*, **26**, 969-990
6. Bergmann G., Graichen F., Rohlmann A., 1995, Is Staircase Walking a Risk for the Fixation of Hip Implants? *J. Biomechanics*, **28**, 535-553
7. Bergmann G., Graichen F., Rohlmann A., 1999, Friction Induced Temperature Increase of Hip Implants, In: L. Sedel and G. Willmann, Edit., *Reliability and Long-Term Results of Ceramics in Orthopaedics*, 91-95, Georg Thieme-Verlag, Stuttgart-New York
8. Bergmann G., Graichen F., Rohlmann A., Linke H., 1997, Hip Joint Forces During Load Carrying, *Clinical Orthop. Related Res.*, **335**, 190-201
9. Chenot J.-L, Bay F., 1998, An Overview of Numerical Modelling Techniques, *J. Mater. Proc. Technology*, **80-81**, 8-15
10. Dowson D., Edit., 1998, *Advances in Medical Tribology*, Mechanical Engineering Publications, London
11. Evans C.H., 1983, Application of Ferrography to the Study of Wear and Arthritis in Human Joints, *Wear*, **90**, 281-292
12. Evans C.H., Bowen E.R., Bowen J., Tew W.P., Westcott V.C., 1980, Synovial Fluid Analysis by Ferrography, *J. Biochem. Biophys. Methods*, **2**, 11-18

13. Evans C.H., Mears D.C., McKnight J.L., 1981, A Preliminary Ferrographic Survey of the Wear Particles in Human Synovial Fluid, *Arthritis and Rheumatism*, **24**, 912-918

14. Evans C.H., Mears D., Stanitski C.L., 1982, Ferrographic Analysis of Wear in Human Joints: Evaluation by Comparison with Arthroscopic Examination of Symptomatic Knee, *J. Bone Joint Surg.*, **64-B**, 572-578

15. Feeny B., Guran A., Hinrichs H., Popp K., 1998, A Historical Review on Dry Friction and Stick-slip Phenomena, *Appl. Mech. Reviews*, **51**, 321-341

16. Fortes M.A., Colaço R., Vaz M. F., 1999, The Contact Mechanics of Cellular Solids, *Wear*, **230**, 1-10

17. García J.R.F., Han W., Shillor M., Sofonea M., 2000, *Recent Advances in Variational and Numerical Analysis of Quasistatic Contact Problems*, Preprint, Departamento de Matematica Aplicada, Universidad de Santiago de Compostela

18. Gibson L., Ashby M., 1988, *Cellular Solids: Structure and Properties*, Pergamon, Oxford

19. Graichen F., Bergmann G., Rohlmann A., 1999, Hip Endoprosthesis for in Vivo Measurement of Joint Force and Temperature, *J. Biomechanics*, **32**, 1113-1117

20. Heegaard J.-H., 1993, Large Slip Contact in Biomechanics: Kinematics and Stress Analysis of the Patello-Femoral Joint, Thèse No 1113, Ecole Polytechnique Fédérale de Lausanne

21. Heegaard J.-H., Curnier A., 1993, An Augmented Lagrangian Method for Discrete Large-Slip Contact Problems, *Int. J. Num. Meth. Eng.*, **36**, 569-593

22. Ingham E., Fischer J., 1999, Wear of Ultra High Molecular Weight Polyethylene in Total Hip Joints, *Biological and Mechanical Mechanisms*, (Preprint)

23. Johansson L., 1992, *Elastic and Thermoelastic Problems with Friction and Wear*, Linköping Studies in Science and Technology, Dissertations, No. 266

24. Joshi M.G., Santare M.H., Advani S.G., 2000, Survey of Stress Analyses of the Femoral Hip Prosthesis, *Appl. Mech. Reviews*, **53**, 1-18

25. Klapperich C., Komvopoulos K., Pruitt L., 1999, Tribological Properties and Microstructure Evolution of Ultra-High Molecular Weight Polyethylene, *ASME J. Tribol.*, **121**, 394-402

26. Kuttler K.L., Shillor M., 1998, *Dynamic Contact Problem with Normal Compliance Wear and Discontinuous Friction Coefficient*, Preprint, Dept. of Mathematical Sciences, Michigan Technological University

27. Laffargue P., Breme H.J., Helsen J.A., Hildebrand H.F., 1998, Retrieval Analysis, In: J.A. Helsen and H.J. Breme, Edit., *Metals as Biomaterials*, 467-501, John Wiley & Sons, Chichester

28. LAURSEN T.A., SIMO J.C., 1993, A Continuum-Based Finite Element Formulation for the Implicit Solution of Multibody, Large Deformation Frictional Contact Problems, *Int. J. Num. Meth. Eng.*, **36**, 3451-3485

29. LIM S.C., ASHBY M.F., 1987, Wear-Mechanism Maps, *Acta Metall.*, **35**, 1, 1-24

30. MACKERLE J., 1998, A Finite Element Bibliography for Biomechanics, *Appl. Mech. Reviews*, **51**, 583-634

31. MAHER S.A., MCCORMACK B.A.O., 1999, Quantification of Interdigitation at Bone Cement/Cancellous Bone Interfaces in Cemented Femoral Reconstructions, *Proc. Inst. Mech. Engrs.*, **213**, Part H, 347-354

32. MEARS D.C., HANLEY E.N., RUTKOWSKI R., 1978, Ferrography: Its Application to the Study of Human Joint Wear, *Wear*, **50**, 115-125

33. MRÓZ Z., STUPKIEWICZ S., 1994, An Anisotropic Friction and Wear Model, *Int. J. Solids and Structures*, **31**, 1113-1131

34. PRENDERGAST P.J., 1997, Finite Element Models in Tissue Mechanics and Orthopaedic Implant Design, *Clinical Biomech.*, **12**, 346-366

35. RAKOTOMANANA L., 2000, The Long-Term Behaviour of Human Joints with Orthopaedic Prosthesis: Finite Element Models, In: *European Congress on Comput. Meth. in Appl. Sci. Eng., ECCOMAS 2000*, Barcelona, 11-14 September, 2000

36. REVELL P.A., AL-SAFFAR N., KOBAYASHI A., 1997, Biological Reaction to Debris in Relation to Joint Prostheses, *Proc. Instn. Mech. Engrs.*, Part H, **211**, 187-197

37. ROCKAFELLER R., WETS R.-B., 1998, *Variational Analysis*, Springer, Berlin

38. ROJEK J., OÑATE E., POSTEK E., 1998, Application of Explicit FE code to Simulation of Sheet and Bulk Metal Forming Processes, *J. Mater. Proc. Technology*, **80-81**, 620-627

39. ROJEK J., TELEGA J.J., 2001, Contact Problems With Friction, Adhesion and Wear in Orthopaedic Biomechanics. Numerical implementation and Application to Implanted Knee Joints. Part I: General Developments, *J. Theor. Appl. Mech.*, **39**, 3

40. SAIKKO V.O., 1993, Wear of Polyethylene Acetabular Cups Against Alumina Femoral Heads, *Acta Orthop. Scand.*, **64**, 507-512

41. SAIKKO V.O., AHLROOS T., 1999, Type of Motion and Lubricant in Wear Simulation of Polyethylene Acetabular Cup, *Proc. Inst. Mech. Engrs.*, **213**, Part H, 301-310

42. SAIKKO V.O., AHLROOS T., 2000, Wear Simulation of UHMWPE for Total Hip Replacement with a Multidirectional Motion Pin-on-Disk Device: Effects of Counterface Material, Contact Area, and Lubricant, *J. Biomed. Mater. Res.*, **49**, 147-154

43. SASAKI S., 1992, Effects of Environment on Friction and Wear of Ceramics, *Bull. Mech. Eng. Laboratories*, **58**

44. SHILLOR M., SOFONEA M., 1999, *A Quasistatic Viscoelastic Contact Problem with Friction*, Preprint, Dept. of Mathematical Sciences, Oakland University

45. STRÖMBERG N., 1997, *Thermomechanical Modelling of Tribological Systems*, Linköping Studies in Science and Technology, Dissertations, No. 497

46. STRÖMBERG N., JOHANSSON L., KLARBRING A., 1996a, Derivation and Analysis of a Generalized Standard Model for Contact, Friction and Wear, *Int. J. Solids and Structures*, **33**, 1817-1836

47. STRÖMBERG N., JOHANSSON L., KLARBRING A., 1996b, A Generalized Standard Model for Contact, Friction and Wear, In: M. Raous, M. Jean, and J.J. Moreau, Edit., *Contact Mechanics*, 327-334, Plenum Press, New York

48. SUH N.P., 1973, The Delamination Theory of Wear, *Wear*, **25**, 111-124

49. SUH N.P., 1977, An Overview of the Delamination Theory of Wear, *Wear*, **44**, 1-16

50. TOKARZEWSKI S., TELEGA J.J., GAŁKA A., 1999, A Contribution to Evaluation of Effective Moduli of Trabecular Bone with Rod-Like Microstructure, *J. Theor. Appl. Mech.*, **37**, 707-728

51. TWORZYDLO W.W., CECOT W., ODEN J.T., YEW C.H., 1998, Computational Micro- and Macroscopic Models of Contact and Friction: Formulation, Approach and Applications, *Wear*, **220**, 113-140

52. UNDERWOOD P.G., 1983, Dynamic Relaxation, In: T. Belytschko and T.J.R. Hughes, Eds, *Computational Methods for Transient Dynamic Analysis*, Amsterdam, North-Holland

53. WALKER P.S., BLUNN G.W., BROOME D.R., PERRY J., WATKINS A., SATHASIVAM S., DEWAR M.E., PAUL J.P., 1997, A Knee Simulating Machine for Performance Evaluation of Total Knee Replacements, *J. Biomechanics*, **30**, 83-89

54. WANG A., ESSNER A., POLINENI V.K., STARK C., DUMBLETON J.H., 1998, Lubrication and Wear of Ultra-High Molecular Weight Polyethylene in Total Joint Replacements, *Tribol. Int.*, **31**, 17-33

55. ZHANG L., TANAKA H., 1997, Towards a Deeper Understanding of Wear and Friction on the Atomic Scale – a Molecular Dynamic Analysis, *Wear*, **211**, 44-53

56. ZIENKIEWICZ O.C., TAYLOR R.L., 1989, *The Finite Element Method*, McGraw-Hill, London

Zagadnienia kontaktowe z tarciem, adhezją i zużyciem w biomechanice ortopedycznej. Część II – Implementacja numeryczna i zastosowanie do stawów kolanowych po implementacji

Streszczenie

Niniejsza praca stanowi część drugą pracy, której autorami są Rojek i Telega (2001). Do analizy interfazy kość-implant zastosowano alternatywny opis adhezji. Opracowano algorytm numeryczny, który zastosowano do analizy stawu kolanowego po endoprotezoplastyce. Zbadano wpływ produktów zużycia na analizowaną interfazę oraz przedstawiono aktualnie stosowane modele zużycia.

Manuscript received February 2, 2001; accepted for print May 23, 2001